Properties of fluorosulfate-based ionic liquids and geometries of $(FO_2SOH)OSO_2F^-$ and $(FO_2SOH)_2O_2SOF^-$

Takeshi Enomoto, Kazuhiko Matsumoto, Rika Hagiwara*

Graduate School of Energy Science, Kyoto University, Yoshida, Sakyo-ku,

Kyoto 606-8501, Japan

* E-mail: k-matsumoto@energy.kyoto-u.ac.jp

Abstract

A room temperature ionic liquid (IL) based on the fluorosulfate anion (SO_3F^-) has been synthesized by the reaction of 1-ethyl-3-methylimidazolium ($EMIm^+$) chloride and fluorosulfuric acid ($HOSO_2F$). The viscosity, ionic conductivity, and electrochemical window of $EMImSO_3F$ at 25 °C are 46.6 mPa s, 10.8 mS cm^{-1}, and 4.3 V, respectively. According to a solvatochromic measurement using ILs, there is a trend in donor ability of fluoro- and oxofluoroanions; $PF_6^- < BF_4^- < N(SO_2CF_3)_2^- < SO_3CF_3^- < SO_3F^- < PO_2F_2^-$, which is explained by the atomic charges obtained from quantum mechanical calculations. The 1:2 and 1:3 stoichiometric reactions of EMImCl and $HOSO_2F$ give $EMIm(FO_2SOH)OSO_2F$ and $EMIm(FO_2SOH)_2O_2SOF$, respectively. Both the salts are liquid at room temperature without a $HOSO_2F$ dissociation pressure (< 1 Pa) and have low viscosity and high ionic conductivity (9.2 mPa s and 30.8 mS cm^{-1} for $EMIm(FO_2SOH)OSO_2F$ and 5.1 mPa s and 43.2 mS cm^{-1} for $EMIm(FO_2SOH)_2O_2SOF$. The vibrational modes and bonding properties of these anionic species are discussed with the aid of quantum mechanical calculations. The $(FO_2SOH)OSO_2F^-$ anion in $EMIm(FO_2SOH)OSO_2F$ does not have an inversion center, which stands in contrast to the one with an inversion center (e.g. observed in solid $Cs(FO_2SOH)OSO_2F$). The $(FO_2SOH)_2O_2SOF^-$ anion in $EMIm(FO_2SOH)_2O_2SOF$ is characterized by vibrational spectroscopy under C_s symmetry.

Electronic supplementary information (ESI) available: Calculated geometrical parameters, NBO charges and bond orders, volumes, $HOSO_2F$ dissociation energies, experimental and calculated vibrational frequencies and intensities, viscosities, ionic conductivities, DSC curves, comparison between the fluorosulfate and fluorohydrogenate ILs, and additional relevant literature.

Introduction

Ionic liquids (ILs) are now widely studied as potential electrolytes for lithium batteries, solar cells, fuel cells, capacitors, and electrolytic bath and environmentally benign media for synthetic and catalytic reactions as well as extraction.[1-8] The properties often observed for ILs are extremely low vapor pressure, non-flammability, high thermal and electrochemical stabilities, and wide temperature range of liquid phase around room temperature.[1-8] Various air-stable ILs have been synthesized and characterized since the reports of BF_4^- and $SO_3CF_3^-$-based ILs.[9, 10] It has been shown in previous works that the size and shape of constituent ions often have a drastic effect on chemical and physical properties of ILs, such as hydrophobicity, polarity, and viscosity. Although some general discussion on such properties can be made based on the anionic species, there are still many unknown factors.

Fluorocomplex anions such as BF_4^- and PF_6^- have been combined with various organic cations to form ILs,[11] whereas oxofluoroanions have not widely been used. Some oxides or oxofluorides have strong fluoride ion acceptor abilities and form chemically and electrochemically stable oxofluoroanions.[12] In our recent report, incorporation of the difluorophosphate anion ($PO_2F_2^-$) resulted in a series of ILs with interesting physical properties (*i.e.* a high ionic conductivity of 12 mS cm^{-1} and a low viscosity of 35 mPa s for $EMImPO_2F_2$ ($EMIm^+$: 1-ethyl-3-methylimidazolium cation)[13]). The asymmetric $PO_2F_2^-$ anion with a large negative charge on the oxygen atoms gives a high donor property to the $PO_2F_2^-$-based ILs. Another interesting candidate as a counter anion in ILs is the fluorosulfate anion (SO_3F^-, see Figure 1). Many inorganic and organic salts based on SO_3F^- have been synthesized and characterized,[14-17] and some of them are commercially available. Although most of the SO_3F^- salts are stable at ambient conditions and $EMImSO_3F$ was reported as reaction media[18], the properties of ILs based on SO_3F^- have not been reported yet. The size of SO_3F^- is larger than that of the tetrafluoroborate anion (BF_4^-), which is a popular anion in ILs, and close to that of the difluorophosphate anion ($PO_2F_2^-$). In terms of molecular symmetry, SO_3F^- has C_{3v} symmetry, lower than that of BF_4^- (T_d), and has a dipole moment as in the case of $PO_2F_2^-$ (C_{2v}).
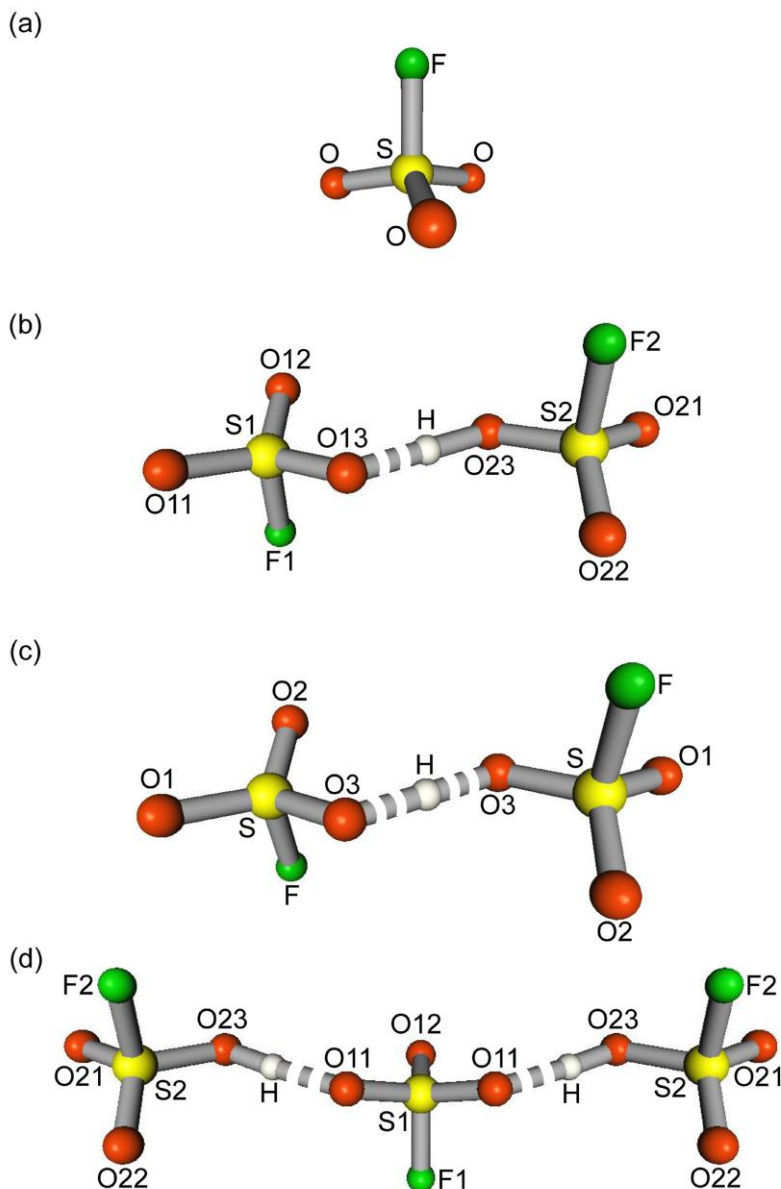
Figure 1. Chemical structures of (a) SO_3F^- (C_{3v}) optimized at B3LYP/aug-cc-pVTZ, (b) $(FO_2SOH)OSO_2F^-$ (C_1) optimized at B3LYP/aug-cc-pVTZ, (c) $(FO_2SOH)OSO_2F^-$ (C_i) optimized at PBE1PBE/aug-cc-pVTZ, and (d) $(FO_2SOH)_2O_2SOF^-$ (C_s) optimized at B3LYP/aug-cc-pVTZ.

The $EMIm^+$ cation has been extensively used in researches of ILs since the ILs based on $EMIm^+$ often exhibit a low melting point and low viscosity with a variety of anions including many fluoroanions.[4, 6, 8, 13, 19-22] This study reports the synthetic procedure and physical and electrochemical properties of the SO_3F-based IL, $EMImSO_3F$. The $HOSO_2F$-rich forms, $EMIm(FO_2SOH)OSO_2F$ and

EMIm(FO$_2$SOH)$_2$O$_2$SOF, which are obtained in a similar way to the case of EMImSO$_3$F are also investigated in the present study. The (FO$_2$SOH)OSO$_2$F$^-$ anion was characterized by spectroscopic and diffractional techniques in previous reports[14, 15] in the solid state, whereas (FO$_2$SOH)$_2$O$_2$SOF$^-$ is unknown to our knowledge. Characterization of these anions in the liquid state gives an interesting insight to understanding these species, which is also done in this paper.

Results and discussion

Synthesis, Computational Results, and Vibrational Spectra. All the three salts, EMIm(FO$_2$SOH)$_n$O$_n$SO$_{3-n}$F (n = 0, 1, and 2), are pale-yellow liquid at room temperature. For the synthesis of EMImSO$_3$F, EMImCl was reacted with excess HOSO$_2$F and the residual HOSO$_2$F was extracted with tri-n-butylphosphate (TBP), followed by washing with tetrahydrofuran. The Cl$^-$ impurity in the resulting EMImSO$_3$F IL was below the detectable level by the AgNO$_3$ test. In the case of the equimolar reaction of EMImCl and HOSO$_2$F, there was residual Cl$^-$ in the liquid after the reaction. Although the Cl$^-$ impurity was reduced to a fairly low level by purification through activated alumina column, a trace of Cl$^-$ was still detected by the AgNO$_3$ test.[13] Thus, the former reaction using excess HOSO$_2$F is preferable to obtain the IL with less Cl$^-$ impurity. The vacuum-stable salts, EMIm(FO$_2$SOH)OSO$_2$F and EMIm(FO$_2$SOH)$_2$O$_2$SOF, were also synthesized by the stoichiometric reaction of EMImCl and HOSO$_2$F, both of them being negative against the AgNO$_3$ test. The 1:3 stoichiometric reaction gives a colorless liquid that is not vacuum-stable and gradually loses HOSO$_2$F under dynamic vacuum, resulting in n = 2 (*i.e.* the HOSO$_2$F content in one mol of the anion reached two mol after 50-day pumping when the synthesis was started from 3.005 g of EMImCl). The salt, EMIm(FO$_2$SOH)$_2$O$_2$SOF, is not air-stable and reacts with moisture in the air, producing HF and H$_2$SO$_4$ as in the case of HOSO$_2$F. On the other hand, there was no visual change when EMIm(FO$_2$SOH)OSO$_2$F was exposed to the air.

The calculated geometrical parameters and molecular volumes of SO$_3$F$^-$, (FO$_2$SOH)OSO$_2$F$^-$, (FO$_2$SOH)$_2$O$_2$SOF$^-$, and HOSO$_2$F at the B3LYP/aug-cc-pVTZ level are listed in Table 1 and compared

5

to those of BF_4^{-}[13] and $PO_2F_2^{-}$[13] in the following discussion (see Tables S1 and S4 in ESI for the results at the other levels with those of $SO_3CF_3^{-}$). Natural bond orbital (NBO)[23-26] charges and bond orders of these species obtained at the B3LYP/aug-cc-pVTZ level are also summarized in Table 1 (see Tables S2 and S3 in ESI for the results at the other levels with those of $SO_3CF_3^{-}$). The overall geometrical parameters of SO_3F^{-} and $(FO_2SOH)OSO_2F^{-}$ agree with those obtained by crystallographic methods although the calculated bond lengths are slightly overestimated.[14] The geometry of SO_3F^{-} was optimized into C_{3v} symmetry in contrast to T_d for BF_4^{-} and C_{2v} for $PO_2F_2^{-}$. The molecular volume of SO_3F^{-} (85 Å^3) is larger than that of BF_4^{-} (77 Å^3) and close to that of $PO_2F_2^{-}$ (85 Å^3). According to the NBO analysis, the fluorine atom in SO_3F^{-} has a charge (-0.573) close to that in BF_4^{-}[13] (-0.572) and slightly less negative than that in $PO_2F_2^{-}$[13] (-0.611), whereas the oxygen atom in SO_3F^{-} is less negatively charged (-0.988) compared to that in $PO_2F_2^{-}$[13] (-1.159).

The geometry of $(FO_2SOH)OSO_2F^{-}$ was optimized under C_1 or C_i symmetry at ten different levels of theory (see Figure 1 and Tables S1 and S6 in ESI for the optimized geometries and vibrational frequencies at the ten levels) and the results differ, depending on the method and basis set. Without any geometrical restriction (C_1), the geometry converged to the higher symmetry, C_i symmetry, at PBE1PBE/cc-pVTZ, PBE1PBE/aug-cc-pVTZ, MPW1PW91/cc-pVTZ, MPW1PW91/aug-cc-pVTZ, and MP2/cc-pVTZ levels, which means that the hydrogen atom is located almost at the inversion center of the molecule. For the calculations at B3LYP/cc-pVTZ, B3LYP/aug-cc-pVTZ, and MP2/aug-cc-pVTZ, the hydrogen atom deviates from the inversion center. Restriction of the geometry within C_i symmetry resulted in the optimized structure with no imaginary frequency at B3LYP/cc-pVTZ, PBE1PBE/aug-cc-pVTZ, MPW1PW91/aug-cc-pVTZ, and MP2/cc-pVTZ levels and one imaginary frequency at B3LYP/aug-cc-pVTZ, PBE1PBE/cc-pVTZ, MPW1PW91/cc-pVTZ, and MP2/aug-cc-pVTZ. As described below, the results of vibrational spectroscopy suggest that $(FO_2SOH)OSO_2F^{-}$ in $EMIm(FO_2SOH)OSO_2F$ belongs to C_1 symmetry, so the following discussion is based on the results at B3LYP/aug-cc-pVTZ level that gave a geometry without an inversion center. The two O−H distances are 1.285 and 1.137 Å and the O−H−O angle of 179.6° in C_1 symmetry, and this calculated geometry

6

differs from the crystallographically determined $(FO_2SOH)OSO_2F^-$ in $Cs(FO_2SOH)OSO_2F^{14}$ (C_i symmetry with the O−H distance of 1.210(2) Å and the O−H−O angle of 180°), which can be caused by the effects of crystal packing. The short O−H−O distance bridged by the hydrogen atom in $(FO_2SOH)OSO_2F^-$ shows existence of the strong interaction between the SO_3F^- and $HOSO_2F$ and supports the negligible vapor pressure of $HOSO_2F$ for the $EMIm(FO_2SOH)OSO_2F$ IL. According to NBO analysis, the atomic charges of oxygen and fluorine atoms in $(FO_2SOH)OSO_2F^-$ are roughly the averaged values of those in SO_3F^- and $HOSO_2F$. The atomic charge of the hydrogen atom in $(FO_2SOH)OSO_2F^-$ (0.517) is similar to that in $HOSO_2F$ (0.513).

The geometry of $(FO_2SOH)_2O_2SOF^-$ is optimized to C_s symmetry (see Figure 1). The hydrogen atom is not optimized at the middle between the two oxygen atoms at any level (the O−H−O angle of 177.1° at B3LYP/aug-cc-pVTZ).

The NBO bond orders for the two O−H bonds in $(FO_2SOH)OSO_2F^-$ (0.424 and 0.305) and in $HOSO_2F$ (0.645) suggest that the O−H bond in $HOSO_2F$ is stronger than that in $(FO_2SOH)OSO_2F^-$, as is expected from their bond length (1.285 and 1.137 Å in $(FO_2SOH)OSO_2F^-$ and 0.970 Å in $HOSO_2F$). The NBO bond orders for the O−H bonds in $(FO_2SOH)_2O_2SOF^-$ are 0.528 and 0.167, and the larger bond order is close to that in $HOSO_2F$. This result as well as the O−H bond lengths of 1.493 and 1.036 Å suggests the interaction between SO_3F^- and $HOSO_2F$ in $(FO_2SOH)_2O_2SOF^-$ anion is weaker than that in $(FO_2SOH)OSO_2F^-$ anion.

Table 1. Calculated geometries, NBO bond orders, NBO charges, and molecular volumes for SO_3F^-, $(FO_2SOH)OSO_2F^-$, $(FO_2SOH)_2O_2SOF^-$ $HOSO_2F$, BF_4^-, and $PO_2F_2^-$ with the geometries of SO_3F^- and $(FO_2SOH)OSO_2F^-$ in the crystal structures of $CsSO_3F$ and $Cs(FO_2SOH)OSO_2F$ [a]

	SO_3F^-		$(FO_2SOH)OSO_2F^-$		$(FO_2SOH)_2O_2SOF^-$	$HOSO_2F$	BF_4^{-b}	$PO_2F_2^{-b}$
	Calcd. (C_{3v})	Obs. (C_1) [c]	Calcd. (C_1)	Obs. (C_i) [d]	Calcd. (C_s)	Calcd. (C_1)	Calcd. (T_d)	Calcd. (C_{2v})
X−F	1.670	1.569(2)	1.631(S1−F1), 1.620(S2−F2)	1.531(2)	1.617(S1−F1), 1.607(S2−F2)	1.589	1.412	1.618
		1.436(2)	1.445(S1−O11), 1.440(S2−O21)	1.399(3)	1.472(S1−O11), 1.435(S2−O21)	1.424(S−O1)		
X−O	1.461	1.437(2)	1.447(S1−O12), 1.441(S2−O22)	1.406(2)	1.443(S1−O12), 1.436(S2−O22)	1.432(S−O2)	-	1.486
		1.458(2)	1.500(S1−O13), 1.519(S2−O23)	1.471(2) [e]	1.544(S2−O23)	1.593(S−O3)		
O−H	-	-	1.285(O13−H), 1.137(O23−H)	1.210(2)	1.493(O11−H), 1.036(O23−H)	0.970	-	-
F−X−F	-	-	-	-	-	-	109.5	95.0
		107.8(2)	103.9(O11−S1−F1), 104.6(O21−S2−F2)	105.3(2)	102.4(O11−S1−F1), 105.4(O21−S2−F2)	106.8(O1−S−F)		
O−X−F	102.0	106.3(1)	103.8(O12−S1−F1), 104.4(O22−S2−F2)	104.8(2)	104.5(O12−S1−F1), 105.1(O22−S2−F2)	106.2(O2−S−F)	-	108.0
		102.3(1)	100.8(O13−S1−F1), 100.5(O23−S2−F2)	101.7(1) [e]	99.9(O23−S2−F2)	98.5(O3−S−F)		
		113.6(1)	119.1(O11−S1−O12), 120.2(O21−S2−O22)	116.3(2)	116.8(O11−S1−O12), 121.7(O21−S2−O22)	124.5(O1−S−O2)		
O−X−O	115.8	112.7(1)	114.2(O12−S1−O13), 114.0(O22−S2−O23)	113.8(1) [f]	111.4(O11−S1−O11) [g], 113.2(O22−S2−O23)	110.2(O2−S−O3)	-	125.6
		113.2(1)	112.2(O13−S1−O11), 110.6(O23−S2−O21)	113.0(2) [f]	108.8(O23−S2−O21)	107.5(O3−S−O1)		
B.O.		-	1.069(S1−O11), 1.081(S2−O21)	-	0.980(S1−O11), 1.097(S2−O21)	0.594(S−O1)	-	-
(X−O) [h]	0.566		1.065(S1−O12), 1.079(S2−O22)		1.075(S1−O12), 1.094(S2−O22)	0.588(S−O2)		
			0.904(S1−O13), 0.856(S2−O23)		0.801(S2−O23)	0.408(S−O3)		
B.O.	-	-	0.305(O13−H), 0.424(O23−H)	-	0.167(O11−H), 0.538(O23−H)	0.645	-	-
(O−H) [h]								

8

Charge (F) [i]	−0.573	-	−0.532(F1), −0.519(F2)	-	−0.516(F1), −0.503(F2)	−0.477	−0.572	−0.611
Charge (O) [i]	−0.988	-	−0.938(O11), −0.925(O21) −0.940(O12), −0.921(O22) −0.961(O13), −0.918(O23)	-	−0.976(O11), −0.904(O21) −0.925(O12), −0.898(O22) −0.889(O23)	−0.877(O1) −0.853(O2) −0.852(O3)	-	−1.159
Charge (X) [i]	2.536	-	2.567(S1), 2.568(S2)	-	2.592(S1), 2.563(S2)	2.546	1.288	2.539
Charge (H) [i]	-	-	0.517	-	0.533	0.513	-	-
Volume	85	-	161	-	231	83	77	85

[a] Bond lengths, bond angles, and molecular volumes are given in Å, deg., and Å^3, respectively. Geometrical parameters and molecular volumes were calculated at B3LYP/aug-cc-pVTZ level. X denotes central atom (S, B, and P) for each molecule. Symbols for the calculated $(FO_2SOH)OSO_2F^-$, $(FO_2SOH)_2O_2SOF^-$ and $HOSO_2F$ are shown in Figure 1. [b] Ref. 13. [c] SO_3F^- (C_1) observed in $CsSO_3F$. Ref. 14. [d] $(FO_2SOH)OSO_2F^-$ (C_i) observed in $Cs(FO_2SOH)OSO_2F$. Ref. 14. [e] The oxygen atom is coordinated by hydrogen atom. [f] One of the two oxygen atoms is coordinated by hydrogen atom. [g] The two O11 oxygen atoms are different atoms [h] NBO bond orders calculated at B3LYP/aug-cc-pVTZ level. [i] NBO charges calculated at B3LYP/aug-cc-pVTZ level.

Raman and infrared (IR) spectra of EMIm(FO$_2$SOH)$_n$O$_n$SO$_{3-n}$F at room temperature are shown in Figure 2. Table 2 shows the vibrational frequencies, intensities, and assignments for SO$_3$F$^-$. The assignments for the vibrational frequencies of SO$_3$F$^-$ are reported in alkali metal fluorosulfate[15, 16], metal bisfluorosulfates[17], and pyridinium fluorosulfate[27]. Here, the spectrum of SO$_3$F$^-$ in EMImSO$_3$F is compared with that in CsSO$_3$F[16], together with the vibrational frequencies and intensities calculated at the B3LYP/aug-cc-pVTZ level in Table 2 (see Table S6 in ESI for the results at the other levels). As a whole, SO$_3$F$^-$ in EMImSO$_3$F exhibits similar vibrational frequencies to those in CsSO$_3$F, whereas small frequency shifts are observed between these two cases. These shifts probably arise from the weaker interaction between the bulky imidazolium cation with delocalized positive charges and SO$_3$F$^-$ compared to the case of the cesium salt. The vibrational frequencies of (FO$_2$SOH)OSO$_2$F$^-$ and (FO$_2$SOH)$_2$O$_2$SOF$^-$ are assigned based on the calculated frequencies of the optimized structures (C_1 and C_s symmetries, respectively), although the calculated modes are quite complicated and some frequencies are assigned to several vibrational modes (see Tables S7-S9 in ESI for the vibrational frequencies and intensities for EMIm(FO$_2$SOH)OSO$_2$F, EMIm(FO$_2$SOH)$_2$O$_2$SOF, and HOSO$_2$F). Some of the vibrational modes of SO$_3$F$^-$ in EMImSO$_3$F are also observed in EMIm(FO$_2$SOH)OSO$_2$F and EMIm(FO$_2$SOH)$_2$O$_2$SOF. For example, the vibrational frequencies around 560 and 1070 cm^{-1} are observed for all the fluorosulfate salts and they are assigned to the δ(SO$_3$) + v(SF) and the v_s(SO$_3$) modes in the case of SO$_3$F$^-$ (557 and 1070 cm^{-1} for Raman frequencies in EMImSO$_3$F). In the Raman spectrum of EMIm(FO$_2$SOH)OSO$_2$F, the latter mode is split into two peaks (1053 and 1067 cm^{-1}). This split implies that the (FO$_2$SOH)OSO$_2$F$^-$ anion in the liquid does not have C_i symmetry unlike the cases of some of the present calculations and crystal structure of Cs(FO$_2$SOH)OSO$_2$F[14] because the (FO$_2$SOH)OSO$_2$F$^-$ under C_i symmetry does not have two Raman active vibrational modes in the range of these frequencies (see Table S6). Violations of the mutual exclusion rule between the Raman and IR spectra also suggest the (FO$_2$SOH)OSO$_2$F$^-$ does not have an inversion center (see Table S7). The frequency around 720 cm^{-1} (the δ(SO$_3$) − v(SF) mode for EMImSO$_3$F) increases as the HOSO$_2$F content of the salts increases due to the strong interaction between the SO$_3$F$^-$ and HOSO$_2$F bridged by hydrogen

atom (the frequencies are around 780 and 800 cm^{-1} for EMIm(FO$_2$SOH)OSO$_2$F and EMIm(FO$_2$SOH)$_2$O$_2$SOF, respectively. *cf.* the value of 840 cm^{-1} for HOSO$_2$F).
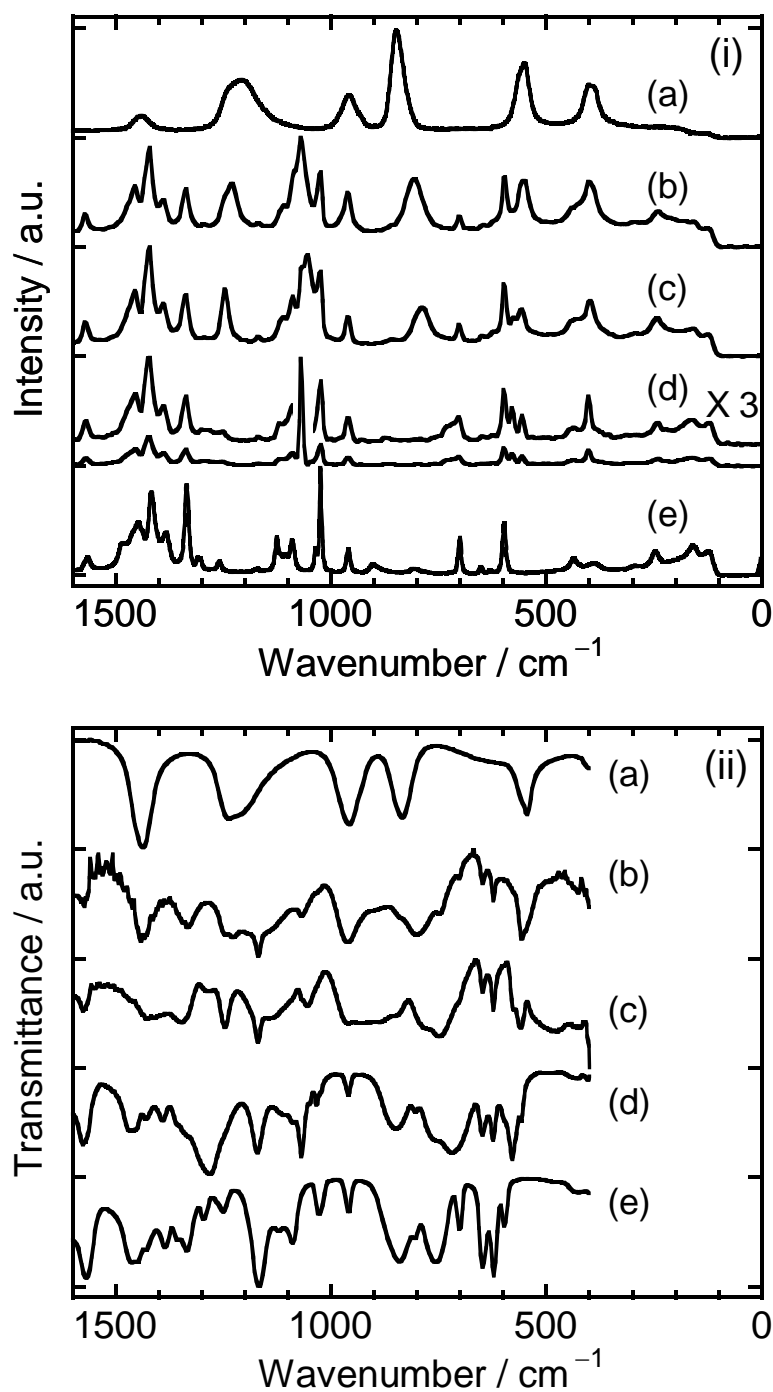
Figure 2. (i) Raman and (ii) IR spectra of (a) HOSO$_2$F (b) EMIm(FO$_2$SOH)$_2$O$_2$SOF (c) EMIm(FO$_2$SOH)OSO$_2$F, (d) EMImSO$_3$F (with the spectrum multiplied by 3 for clarity in the Raman spectrum), and (e) EMImCl.

Table 2. Vibrational frequencies, intensities, and assignments for SO_3F^{-} [a]

EMImSO$_3$F [b]		CsSO$_3$F [c]			
Raman	IR	Raman	IR	Calcd. [d]	Assignment [e] (C_{3v})
402(15)	403(w)	409	416	369(2)[<1]	$\delta(SO_2) + \delta(S(F)O)$
557(9)	558(w)	560	558	508(5)[3]	$\delta(SO_3) + \nu(SF)$
580(11)	579(s)	588	578	549(2)[30]	$\delta(S(F)O_2)$
			585		
730(6)	719(m)	728	715	665(6)[269]	$\delta(SO_3) - \nu(SF)$
1070(100)	1069(s)	1079	1078	1028(43)[60]	$\nu_s(SO_3)$
1291(4)	1281(s)	1285	1295	1256(7)[374]	$\nu_a(SO_3)$
n.d.	1650(sh)	n.d.	1662		combination
n.d.	2352(sh)	n.d.	2365		combination

[a] Frequencies are given in cm^{-1}. [b] Liquid at 25°C. The experimental Raman intensities are scaled relative to the intensity of the $\nu_s(SO_3)$ mode of SO_3F^{-}, which is assigned to a value of 100. The abbreviations, sh, w, m, and s, denote shoulder, weak, medium, and strong. [c] Ref 16. [d] B3LYP/aug-cc-pVTZ. Values in parentheses are Raman intensities (Å^4 amu^{-1}) and values in square brackets are infrared intensities (km mol^{-1}). [e] ν: stretching. δ: bending or deformation. Subscripts, a and s, denote asymmetric and symmetric modes, respectively.

Physical and chemical properties. Selected physical properties of EMIm(FO$_2$SOH)$_n$O$_n$SO$_{3-n}$F ($n = 0$, 1, 2) are listed in Table 3 with those of EMImBF$_4$[28], EMImPO$_2$F$_2$[13], EMImSO$_3$CF$_3$[10], and EMIm(FH)$_{2.3}$F[29].

Differential scanning calorimetry (scan rate of 5°C min^{-1}) revealed that all the three EMIm(FO$_2$SOH)$_n$O$_n$SO$_{3-n}$F salts do not show a melting point (above around −140°C), although EMImSO$_3$F and EMIm(FOSO$_2$H)OSO$_2$F show glass transition at −95°C and −121°C, respectively (Figure S1 in ESI for the DSC curves).

Table 3. Physical properties of selected ILs [a]

IL	FW	T_m (T_g) / °C	ρ / g cm^{-3}	MV / cm^3 mol^{-1}	η / mPa s	σ / mS cm^{-1}	Λ / S cm^2 mol^{-1}
EMImSO$_3$F	210	(−95)	1.32	159	46.6	10.8	1.7
EMIm(FO$_2$SOH)OSO$_2$F	310	(−121)	1.40	221	9.2	30.8	6.8
EMIm(FO$_2$SOH)$_2$O$_2$SOF	410	n.d.	1.46	281	5.1	43.2	12.1
EMImBF$_4$ [b]	198	15	1.28	155	34	13.0	2.0
EMImPO$_2$F$_2$ [c]	212	7	1.31	162	35	12	1.9
EMImSO$_3$CF$_3$ [d]	260	-	1.38	188	42.7	9.3	1.7
EMIm(FH)$_{2.3}$F [e]	176	−65	1.13	156	4.9	100	15.6

[a] FW: formula weight, T_m: melting point, T_g: glass transition temperature, ρ: density at 25°C, MV: molar volume at 25°C, η: viscosity at 25°C, σ: ionic conductivity at 25°C, Λ: molar conductivity at 25°C. [b] Ref. 27. [c] Ref. 13. [d] Ref. 10. [e] Ref. 28.

Thermogravimetric curves for EMIm(FO$_2$SOH)$_n$O$_n$SO$_{3-n}$F salts (scan rate of 10°C min^{-1}) are shown in Figure 3. Thermal decomposition temperatures defined as the temperature where the salt loses 5% of its weight are 330, 200, and 160°C for EMImSO$_3$F, EMIm(FO$_2$SOH)OSO$_2$F, and EMIm(FO$_2$SOH)$_2$O$_2$SOF, respectively. The decomposition temperature of EMImSO$_3$F seems to be reasonable compared to those of other EMIm salts[13, 30], whereas EMIm(FO$_2$SOH)OSO$_2$F and EMIm(FO$_2$SOH)$_2$O$_2$SOF gradually lose their weights at lower temperatures compared to EMImSO$_3$F. If the stoichiometric amount of HOSO$_2$F is eliminated from these salts, the weight loss for EMIm(FO$_2$SOH)OSO$_2$F is 32% and that for EMIm(FO$_2$SOH)$_2$O$_2$SOF is 24 (1st HOSO$_2$F) and 49% (2nd HOSO$_2$F). However, obvious plateaus were not observed in the thermogravimetric curves probably because the decomposition involving the cation occurs under the present condition before complete evaporation of the stoichiometric amount of HOSO$_2$F.
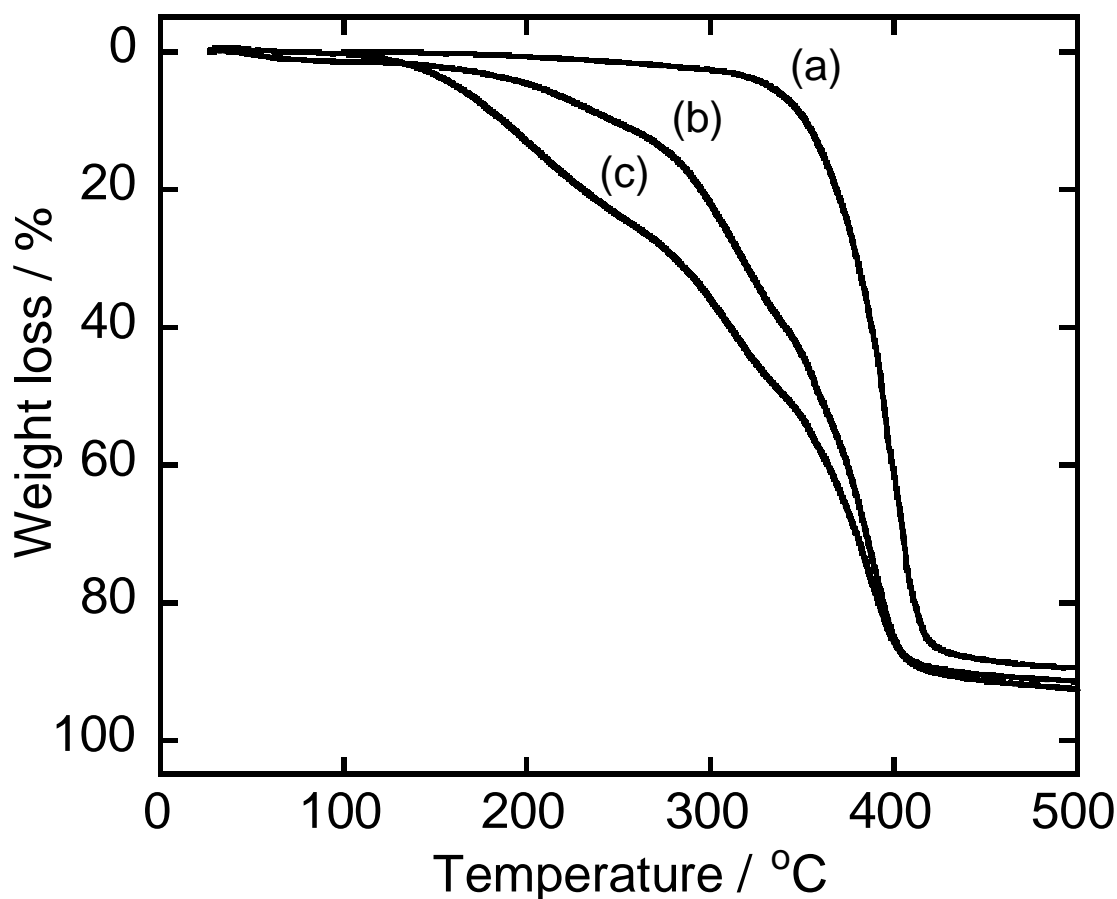
Figure 3. Thermogravimetric curves for $EMIm(FO_2SOH)_nO_nSO_{3-n}F$ (n = 0, 1, and 2); (a) $EMImSO_3F$, (b) $EMIm(FO_2SOH)OSO_2F$, and (c) $EMIm(FO_2SOH)_2O_2SOF$. Scan rate of 10^oC min^{-1} was used.

Arrhenius plot of viscosity for $EMImSO_3F$ and those of ionic conductivity for $EMIm(FO_2SOH)_nO_nSO_{3-n}F$ (n = 0, 1, and 2) are shown in Figure 4. $EMImSO_3F$ exhibits a viscosity of 46.6 mPa s at 25^oC. This value is larger than those of $EMImBF_4$ (34 mPa s)[28] and $EMImPO_2F_2$ (35 mPa s)[13] and close to that of $EMImSO_3CF_3$ (42.7 mPa s)[10]. The ionic conductivity of 10.8 mS cm^{-1} for $EMImSO_3F$ at 25^oC is slightly smaller than those of $EMImBF_4$ (13.0 mS cm^{-1})[28] and $EMImPO_2F_2$ (12 mS cm^{-1})[13]. Since the Walden's law ($\eta \cdot \Lambda$ = constant)[19, 21, 31-33] is roughly applicable to ILs, the similar viscosities of $EMImSO_3F$ and $EMImSO_3CF_3$[10] lead to their similar molar conductivity. The larger ionic conductivity of $EMImSO_3F$ than that of $EMImSO_3CF_3$[10] simply reflects the difference in the number of ions per volume.

The viscosities and ionic conductivities at 25°C are 9.2 mPa s and 30.8 mS cm^{-1} for EMIm(FO$_2$SOH)OSO$_2$F and 5.1 mPa s and 43.2 mS cm^{-1} for EMIm(FO$_2$SOH)$_2$O$_2$SOF, respectively. These viscosity and conductivity values are quite low and high, respectively, compared to popular ILs. The viscosity and ionic conductivity of EMIm(FO$_2$SOH)$_n$O$_n$SO$_{3-n}$F (n = 0, 1, and 2) decreases and increases, respectively, with increase in n. The low viscosity and high ionic conductivity of ILs containing (FO$_2$SOH)OSO$_2$F$^-$ and (FO$_2$SOH)$_2$O$_2$SOF$^-$ have some similarities with those of fluorohydrogenate ((FH)$_n$F$^-$) ILs, where the molecular unit (HOSO$_2$F or HF) is considered to work as a dielectric spacer to weaken cation-anion interactions (see ESI for comparison of these two systems).[34, 35] The molar conductivity of EMIm(FO$_2$SOH)$_2$O$_2$SOF is slightly lower than that of EMIm(FH)$_{2.3}$F, whereas the ionic conductivity of EMIm(FO$_2$SOH)$_2$O$_2$SOF is not as large as that of EMIm(FH)$_{2.3}$F because the number of ions per volume for EMIm(FO$_2$SOH)$_2$O$_2$SOF is smaller than that of EMIm(FH)$_{2.3}$F.

The Arrhenius plots show nearly linear dependence in the measured temperature range (5-75°C) and activation energies calculated from the plots are listed in Table 4. The activation energies of ionic conductivity decrease in the order of EMImSO$_3$F > EMIm(FO$_2$SOH)OSO$_2$F > EMIm (FO$_2$SOH)$_2$O$_2$SOF with increase of n. The exchange of the HOSO$_2$F unit between the anions is highly probable in EMIm(FO$_2$SOH)OSO$_2$F and EMIm(FO$_2$SOH)$_2$O$_2$SOF as in the case of fluorohydrogenate ILs and the exchanging unit can work as a dielectric spacer to reduce the viscosity and thus conductivity of these ILs.[34, 35]

The Walden products (in [S cm^2 mol^{-1}][mPa s]) of 79, 63, and 62 for EMImSO$_3$F, EMIm(FO$_2$SOH)OSO$_2$F, and EMIm(FO$_2$SOH)$_2$O$_2$SOF are close to those for other known ILs (*e.g.* 76 for EMIm(FH)$_{2.3}$F[29], 68 for EMImBF$_4$[28], 67 for EMImPO$_2$F$_2$[13], and 73 for EMImSO$_3$CF$_3$[10]), which suggests that there is no special conduction mechanism such as Grotthuss hopping mechanism in EMIm(FO$_2$SOH)OSO$_2$F and EMIm(FO$_2$SOH)$_2$O$_2$SOF.
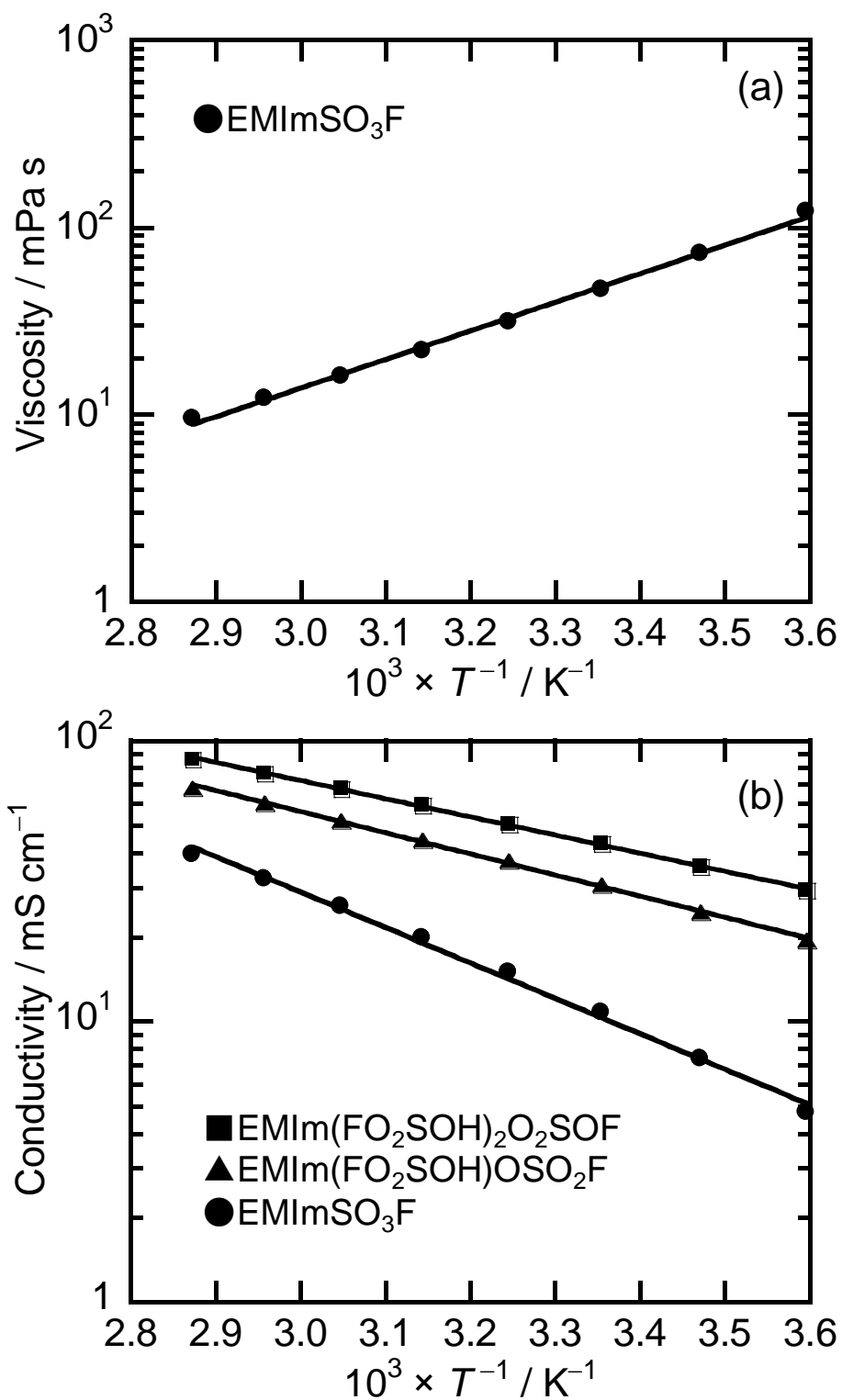
Figure 4. Arrhenius plots of (a) viscosity for EMImSO$_3$F and (b) ionic conductivity for EMIm(FO$_2$SOH)$_n$O$_n$SO$_{3-n}$F (n = 0, 1, and 2).

Table 4. Activation energies of viscosity and ionic conductivity for EMIm(FO$_2$SOH)$_n$O$_n$SO$_{3-n}$F ($n = 0$, 1, and 2)[a]

Activation energy	EMImSO$_3$F	EMIm(FO$_2$SOH)OSO$_2$F	EMIm(FO$_2$SOH)$_2$O$_2$SOF
$E_a(\eta)$ / kJ mol^{-1}	29.3	-	-
$E_a(\sigma)$ / kJ mol^{-1}	24.2	14.4	12.4

[a] $E_a(\eta)$ and $E_a(\sigma)$: activation energies of viscosity and ionic conductivity, respectively.

Although the polarity of ionic liquids is not easy to evaluate by a single method,[36] the donor property of EMImSO$_3$F was evaluated by a solvatochromic method using a square planar complex salt, [Cu(tmen)(acac)][BPh$_4$] (tmen = *N,N,N',N'*-tetramethylethylenediamine, acac = acetylacetonate, and BPh$_4$ = tetraphenylborate) in this study. This is because the effect of the anion was an object of interest and this dye is useful for this purpose. The Cu(tmen)(acac)$^+$ cation shows an absorption peak for the lowest energy *d-d* band in the visible range and the position of the maximum wavelength (λ_{Cu}) depends on the donor property of the anionic species in the ILs regardless of the cationic structure.[13, 37] Figure 5 shows visible absorption spectra of [Cu(tmen)(acac)][BPh$_4$] in EMImSO$_3$F together with those in EMImBF$_4$[13] and EMImPO$_2$F$_2$[13]. The λ_{Cu} value obtained for SO$_3$F$^-$ (589 nm for EMImSO$_3$F) is between the values of BF$_4^-$ (537 nm for EMImBF$_4$[13]) and PO$_2$F$_2^-$ (625 nm for EMImPO$_2$F$_2$[13]). The results of quantum mechanical calculations discussed above indicate that the oxygen atoms in SO$_3$F$^-$ and PO$_2$F$_2^-$ have a negative charge twice as large as that of the fluorine atoms and can strongly interact with the copper center, resulting in a larger λ_{Cu} value than that in BF$_4^-$. Furthermore, the lower λ_{Cu} value for SO$_3$F$^-$ than that of PO$_2$F$_2^-$ could be derived from its less negative charges of the oxygen atoms in SO$_3$F$^-$ than that in PO$_2$F$_2^-$. The λ_{Cu} value for SO$_3$F$^-$ is slightly larger than that for SO$_3$CF$_3^-$ (579 nm for BMImSO$_3$CF$_3$[37]). Since the NBO charge on the oxygen atom in SO$_3$CF$_3^-$ (−0.993 at B3LYP/aug-cc-pVTZ level. See Table S2 in ESI for the results at the other levels) is close to that in SO$_3$F$^-$, the weaker donor property of SO$_3$CF$_3^-$ may arise from the steric effect. Comparing the λ_{Cu} values for some fluoro-

and oxofluorocomplex anions give the following order in donor ability; PF_6^- < BF_4^- < $N(SO_2CF_3)^-$ < $SO_3CF_3^-$ < SO_3F^- < $PO_2F_2^-$.[13, 37]
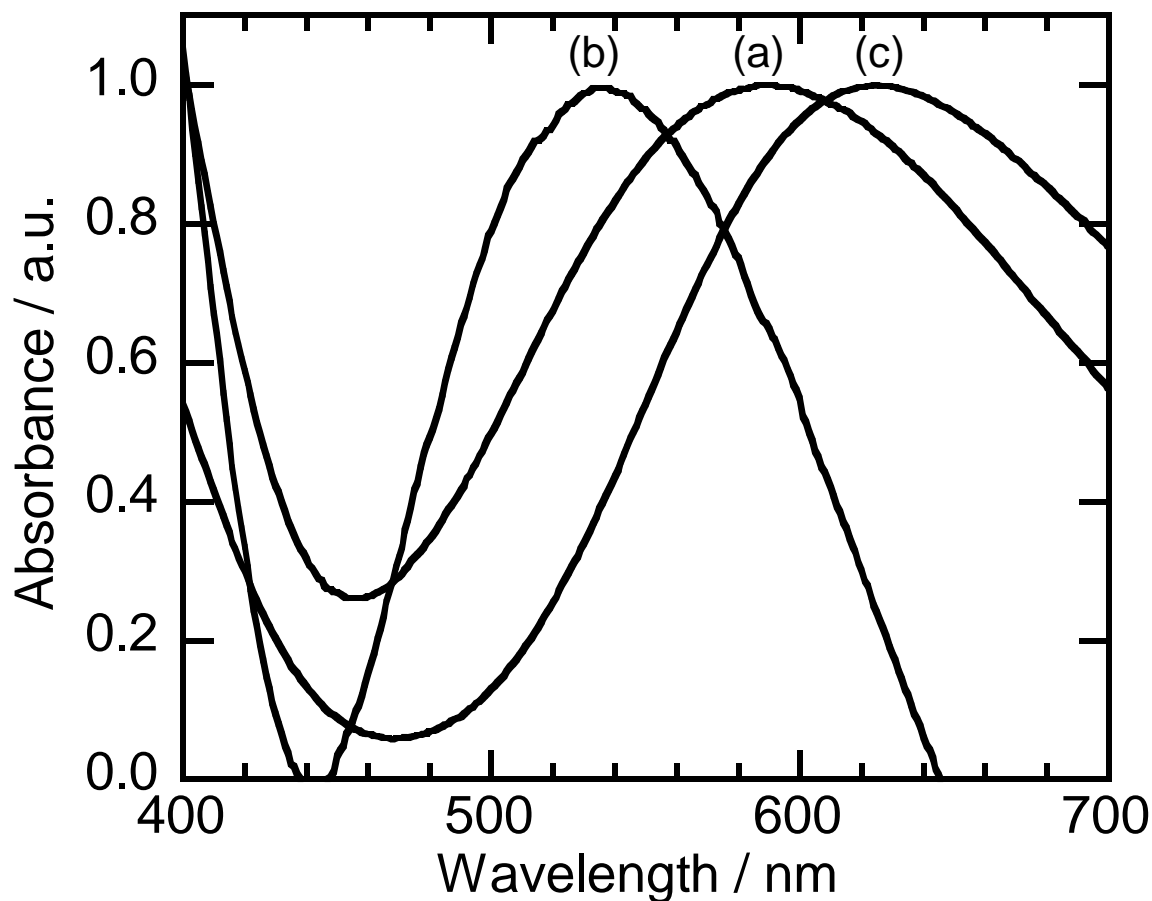

Figure 5. Visible absorption spectra of EMIm-based ILs containing 0.01 M of [Cu(tmen)(acac)][BPh$_4$]. (a) EMImSO$_3$F, (b) EMImBF$_4$, and (c) EMImPO$_2$F$_2$. For (b) EMImBF$_4$ and (c) EMImPO$_2$F$_2$, see ref. 13.

Electrochemical properties. Linear sweep voltammograms of glassy carbon and platinum electrodes in EMIm(FO$_2$SOH)$_n$O$_n$SO$_{3-n}$F salts are shown in Figure 6. Electrochemical windows of EMIm(FO$_2$SOH)$_n$O$_n$SO$_{3-n}$F salts with glassy carbon and platinum electrodes are listed in Table 5. The redox potential of Fc$^+$/Fc in EMImSO$_3$F was −0.66 V *vs.* Ag$^+$/Ag and the potential was not measured in EMIm(FO$_2$SOH)OSO$_2$F and EMIm(FO$_2$SOH)$_2$O$_2$SOF because the HOSO$_2$F unit in the anion seemed to react with ferrocene. The anode and cathode limits are determined as the potentials where the absolute values of the current densities exceed 0.5 mA cm^{-2} at the scan rate of 10 mV s^{-1}. EMImSO$_3$F, exhibits

an electrochemical window of 4.3 V on a glassy carbon electrode (4.1 V for a platinum electrode) which is comparable to that of EMImPO$_2$F$_2$[13] and slightly smaller than that of EMImBF$_4$.[30, 38, 39] The cathode and anode limits of this IL are −3.12 V and 1.20 V vs. Ag$^+$/Ag, respectively. The electrochemical windows of EMIm(FO$_2$SOH)OSO$_2$F (2.0 V for a glassy carbon electrode) and EMIm(FO$_2$SOH)$_2$O$_2$SOF (2.2 V for a glassy carbon electrode) are significantly narrower than that of EMImSO$_3$F due to the hydrogen gas evolution from the anions at the cathode limits. The cathode limits of EMIm(FO$_2$SOH)OSO$_2$F and EMIm(FO$_2$SOH)$_2$O$_2$SOF on a platinum electrode are more positive (0.01 and 0.16 V vs. Ag$^+$/Ag, respectively) than those on a glassy carbon electrode (−0.61 and −0.58 V vs. Ag$^+$/Ag, respectively) because of the low overpotential for hydrogen gas evolution on a platinum electrode. The anode limits of EMIm(FO$_2$SOH)$_n$O$_n$SO$_{3-n}$F salts shift from 1.2 to 1.6 V vs. Ag$^+$/Ag for both the glassy carbon and platinum electrodes in the order of EMImSO$_3$F < EMIm(FO$_2$SOH)OSO$_2$F < EMIm(FO$_2$SOH)$_2$O$_2$SOF. This order of the anodic stability can be explained by the calculated highest occupied molecular orbital energy (E_{HOMO}) at HF/aug-cc-pVTZ and vertical ionization potential (ΔE_v) of the anionic species at B3LYP/aug-cc-pVTZ.[13, 40-43] The E_{HOMO} and ΔE_v of SO$_3$F$^-$, (FO$_2$SOH)OSO$_2$F$^-$, and (FO$_2$SOH)$_2$O$_2$SOF$^-$ are listed in Table 6 and the order of their levels is qualitatively consistent with each other. The lower anodic stability of fluorosulfate ILs reflects the higher E_{HOMO} and larger ΔE_v of the anionic species.
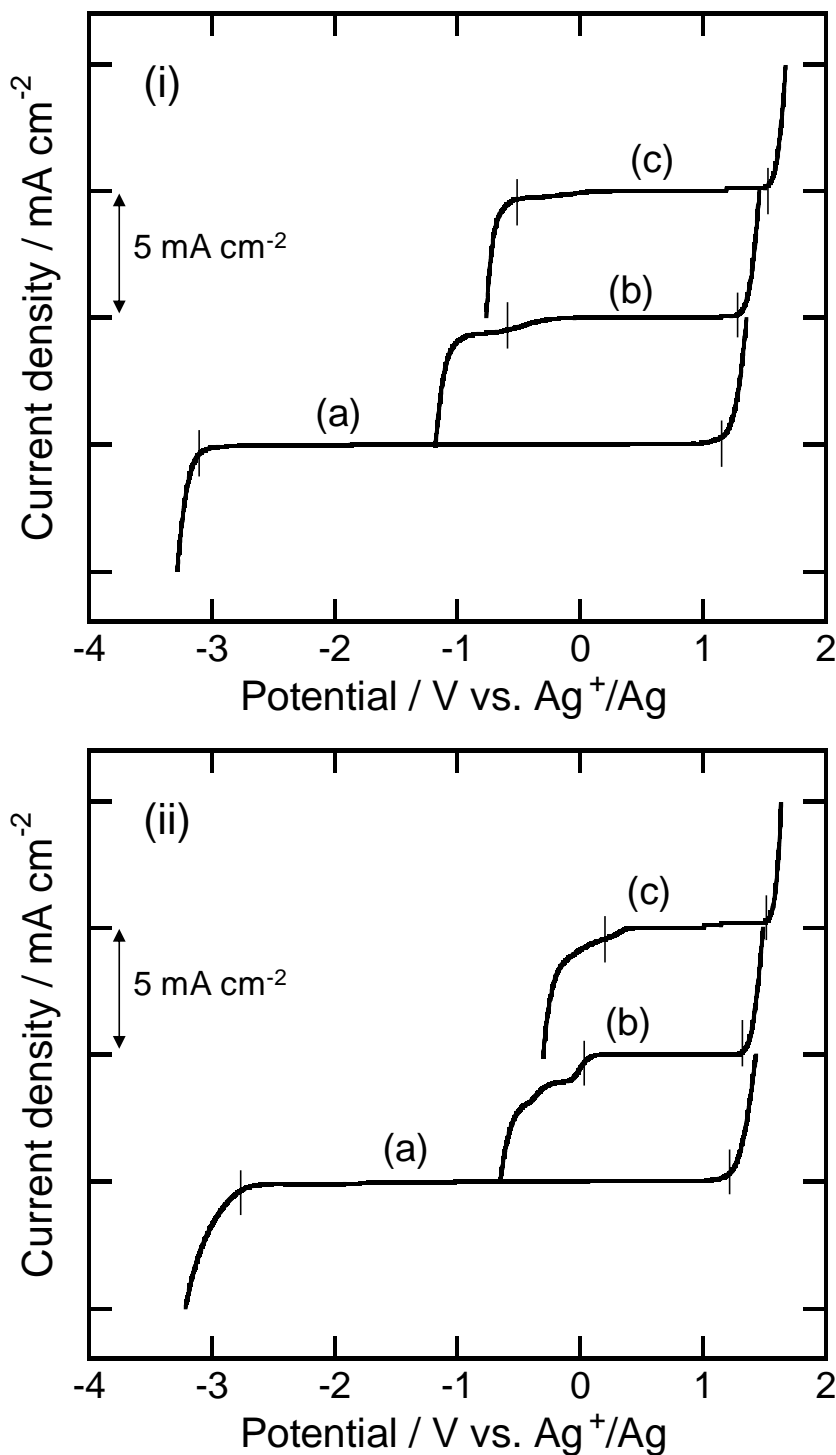
Figure 6. Linear sweep voltammograms of (i) glassy carbon and (ii) platinum electrodes in EMIm(FO$_2$SOH)$_n$O$_n$SO$_{3-n}$F (n = 0, 1, and 2); (a) EMImSO$_3$F, (b) EMIm(FO$_2$SOH)OSO$_2$F, and (c) EMIm(FO$_2$SOH)$_2$O$_2$SOF. Vertical lines denote the anode and cathode limits determined as the potentials where the absolute values of the current densities exceed 0.5 mA cm^{-2} at the scan rate of 10 mV s^{-1}.

Table 5 Electrochemical windows of EMIm(FO$_2$SOH)$_n$O$_n$SO$_{3\text{-}n}$F (n = 0, 1, and 2) [a]

IL	Glassy carbon electrode		Platinum electrode	
	E_{ca} / V	E_{an} / V	E_{ca} / V	E_{an} / V
EMImSO$_3$F	−3.12	1.20	−2.81	1.25
EMIm(FO$_2$SOH)OSO$_2$F	−0.61	1.34	0.01	1.37
EMIm(FO$_2$SOH)$_2$O$_2$SOF	−0.58	1.57	0.16	1.55

[a] E_{ca} and E_{an}: anode and cathode limits, respectively. Potentials were referenced to the Ag$^+$/Ag redox potential. The redox potential of Fc$^+$/Fc in EMImSO$_3$F was −0.66 V *vs*. Ag$^+$/Ag.

Table 6 E_{HOMO} and ΔE_v for (FO$_2$SOH)$_n$O$_n$SO$_{3\text{-}n}$F$^-$ (n = 0, 1, and 2) [a]

Molecule	E_{HOMO} / eV	ΔE_V / eV
SO$_3$F$^-$ (C_{3v})	−7.0	−5.3
(FO$_2$SOH)OSO$_2$F$^-$ (C_1)	−8.6	−6.8
(FO$_2$SOH)$_2$O$_2$SOF$^-$ (C_s)	−9.7	−7.5

[a] E_{HOMO} and ΔE_V was calculated at HF/aug-cc-pVTZ and B3LYP/aug-cc-pVTZ, respectively.

Conclusion

New fluorosulfate-based ILs were synthesized and their spectroscopic, physical, chemical, and electrochemical properties were investigated. The three salts, EMImSO$_3$F, EMIm(FO$_2$SOH)OSO$_2$F, and EMIm(FO$_2$SOH)$_2$O$_2$SOF, are vacuum-stable liquids at room temperature. The anions in these salts were characterized by spectroscopic methods as well as quantum mechanical calculations. For (FO$_2$SOH)OSO$_2$F$^-$ and (FO$_2$SOH)$_2$O$_2$SOF$^-$, some shifts of vibrational modes with respect to that of SO$_3$F$^-$ were observed due to the strong interaction between the SO$_3$F$^-$ and HOSO$_2$F. Vibrational

spectroscopy revealed that the hydrogen atom in $(FO_2SOH)OSO_2F^-$ is not placed at the inversion center. The viscosity of $EMImSO_3F$ is relatively low compared to other EMIm-based ILs. The viscosities and ionic conductivities of $EMIm(FO_2SOH)_nO_nSO_{3-n}F$ ($n = 0, 1,$ and 2) decrease and increase, respectively, with increase in the n value. Thermogravimetry shows no obvious weight loss below 300^oC for $EMImSO_3F$ and 100^oC for $EMIm(FO_2SOH)OSO_2F$ and $EMIm(FO_2SOH)_2O_2SOF$. According to the solvatochromic method, the donor ability of SO_3F^- in $EMImSO_3F$ is between BF_4^- and $PO_2F_2^-$, which is explained by the calculated negative charge on the oxygen and fluorine atoms in these anions. The electrochemical windows of $EMImSO_3F$ is 4.3 V and comparable to that of $EMImPO_2F_2$ and slightly smaller than that of $EMImBF_4$, whereas those of $EMIm(FO_2SOH)OSO_2F$ and $EMIm(FO_2SOH)_2O_2SOF$ are much narrower because of hydrogen gas evolution at the cathode limits.

Experimental

Apparatus and Materials. Moisture sensitive materials were handled in a glove box. A vacuum line was constructed of stainless steel to handle corrosive gases. The line was connected to a rotary vacuum pump through a soda lime chemical trap connected to a glass cold trap in series. A T-shaped reactor made of tetrafluoroethylene-perfluoroalkylvinylether copolymer (PFA) tubes and a polytetrafluoroethylene (PTFE) union was used for the reactions. The precursor, 1-ethyl-3-methylimidazolium chloride (EMImCl) (Yoyu Lab.), was purified by recrystallization from the acetonitrile (Wako Pure Chemical Industries, Ltd., purity $\geq$ 99%, water content $\leq$ 50 ppm) solution by adding ethyl acetate (Wako Pure Chemical Industries, Ltd., purity $\geq$ 99.5%, water content $\leq$ 50 ppm), and dried under vacuum in a Pyrex glass container around 80^oC for a few days prior to use. Fluorosulfuric acid ($HOSO_2F$) (Sigma-Aldrich Co., purified by triple-distillation), tri-n-butyl phosphate (TBP) (Wako Pure Chemical Industries, Ltd., purity $\geq$ 97.0%), and tetrahydrofuran (THF) (Wako Pure Chemical Industries, Ltd., purity $\geq$ 99.5%, water content $\leq$ 50 ppm) were used as purchased.

Synthesis of $EMImSO_3F$ (Method I). Two synthetic methods were attempted for $EMImSO_3F$. The first one was the equimolar reaction of EMImCl with $HOSO_2F$ followed by purification through

activated alumina column[13]. Under a dry argon atmosphere, 7.563 g of EMImCl (51.58 mmol) was loaded in one end of a PFA T-shaped reactor and 5.162 g of $HOSO_2F$ (51.58 mmol) was loaded in the other end. The reactor was connected to the vacuum line and $HOSO_2F$ was slowly added to EMImCl at 0^oC under static vacuum. The byproduct, HCl was occasionally removed by pumping and the volatile materials were evacuated at room temperature after the reaction ceased. Removal of volatiles at 80^oC for one day gave a crude $EMImSO_3F$ sample. The crude $EMImSO_3F$ was dissolved into acetone and purified by column chromatography through an activated alumina (Wako Pure Chemical Industries, Ltd., 75 μm) column. The solvent was initially removed under vacuum at room temperature and then at 80^oC for one day. Testing for the presence of residual chloride impurities with aqueous silver nitrate ($AgNO_3$) gave little precipitation of AgCl. The water content measured by Karl-Fisher titration was below 100 ppm. Anal. Calcd. for $C_6H_{11}N_2S_1O_3F_1$: C, 34.28; H, 5.27; N, 13.33; S, 15.25; F, 9.04. Found: C, 34.03; H, 5.38; N, 13.33; S, 14.96; F, 8.76.

Synthesis of EMImSO₃F (Method II). The $HOSO_2F$-excess salt, $EMIm(FO_2SOH)_nO_nSO_{3-n}F$, was synthesized by the reaction of EMImCl with excess $HOSO_2F$. Under a dry argon atmosphere, 7.047 g of EMImCl (48.06 mmol) was loaded in one end of a PFA T-shaped reactor and 9.738 g of $HOSO_2F$ (97.31 mmol) was loaded in the other end. The reactor was connected to the vacuum line and $HOSO_2F$ was slowly added to EMImCl at 0^oC under static vacuum. The byproduct, HCl, was occasionally evacuated by pumping and the sample was evacuated at room temperature and successively at 60^oC overnight. The prepared sample, $EMIm(FO_2SOH)_nO_nSO_{3-n}F$ (14.98 g, $n = 1.01$. This n value was determined by weight change.) was loaded in a PFA reactor and $HOSO_2F$ in the salt was extracted by TBP until the TBP phase reached neutral in pH. After washing the resulting IL by THF to remove TBP, volatiles were removed initially under vacuum at room temperature and then at 60^oC for one day. The final product (5.757 g, 27.38 mmol, yield: 57%) showed no AgCl precipitation after adding aqueous $AgNO_3$. Anal. Calcd. for $C_6H_{11}N_2S_1O_3F_1$: C, 34.28; H, 5.27; N, 13.33; S, 15.25; F, 9.04. Found: C, 34.34; H, 5.13; N, 13.39; S, 15.16; F, 8.91.

Synthesis of EMIm(FO₂SOH)OSO₂F. The salt, $EMIm(FO_2SOH)OSO_2F$, was synthesized by the

stoichiometric reaction of EMImCl with $HOSO_2F$. Under a dry argon atmosphere, 5.585 g of EMImCl (38.09 mmol) was loaded in one end of a PFA T-shaped reactor and 7.627 g of $HOSO_2F$ (76.22 mmol) was loaded in the other end. The reactor was connected to the vacuum line and $HOSO_2F$ was slowly added to EMImCl at 0^oC under static vacuum. The byproduct, HCl, was occasionally evacuated by pumping and the sample was evacuated at room temperature after the reaction ceased. Further pumping at 60^oC for one day was required for complete removal of HCl from the product $EMIm(FO_2SOH)OSO_2F$ (11.72 g, 37.77 mmol). The sample showed no AgCl precipitation after adding aqueous $AgNO_3$.

Synthesis of $EMIm(FO_2SOH)_2O_2SOF$. The salt, $EMIm(FO_2SOH)_2O_2SOF$, was synthesized by the stoichiometric reaction of EMImCl (4.246 g, 28.96 mmol) with $HOSO_2F$ (8.697 g, 86.91 mmol) in the same manner as for $EMIm(FO_2SOH)OSO_2F$. The final product of $EMIm(FO_2SOH)_2O_2SOF$ (11.82 g, 28.80 mmol) was obtained by evacuating the sample at room temperature for one day. The sample showed no AgCl precipitation after adding aqueous $AgNO_3$.

Analysis. Phase transition temperatures were determined by a differential scanning calorimeter, DSC-60 (Shimadzu Corp.) under a dry argon gas flow (50 mL min^{-1}). Samples were sealed in stainless steel cells using a high-pressure sealing machine in a glove box. A scan rate of 5^oC min^{-1} was used in the present study. Thermal decomposition temperatures were measured by a thermogravimetric analyzer, DTG-60H (Shimadzu Corp.) under a dry argon gas flow (50 mL min^{-1}). Platinum cells used for the measurement were washed with acetone just before the measurement and dried in the apparatus at 200^oC for 10 minutes. The temperature was scanned from room temperature to 500^oC with a heating rate of 10^oC min^{-1}. Electrochemical stability of ILs was investigated by linear sweep voltammetry under a dry argon atmosphere with the aid of HZ-3000 (Hokuto Denko Corp.) electrochemical measurement system. Glassy carbon electrodes (Tokai Carbon Co., Ltd.) with a surface area of 0.07 cm^2 and 0.20 cm^2 were used as working and counter electrodes, respectively. A silver wire immersed in $EMlmBF_4$ containing 0.05 M $AgBF_4$ was used for the reference electrode and was partitioned in the electrolyte with a porous PTFE filter. A platinum plate (Nilaco Corp. 0.1 mm thickness) with a surface area of 0.15

cm^2 was also used as a working electrode. Ionic conductivity was measured by an AC impedance technique with the aid of VSP (Bio-Logic) electrochemical measurement system using a cell with platinum disk electrodes calibrated by KCl standard aqueous solutions. Viscosity was measured by a cone and plate rheometer, LVDV-II+Pro (Brookfield Engineering Laboratories, Inc.) with a CPE-40 spindle for EMImSO$_3$F. The sample was enclosed in the apparatus under a dry argon atmosphere in a glove bag. A hand-made PFA Ostwald viscometer was also used for the viscosity measurements at room temperature for EMIm(FO$_2$SOH)OSO$_2$F and EMIm(FO$_2$SOH)$_2$O$_2$SOF because of their corrosivity. Density was measured by weighing the sample in a calibrated PFA vessel. Raman spectra were obtained by a Raman spectrometer, FTS-175C (Bio-Rad Laboratories, Inc.) at room temperature using the 1064 nm line of a Nd:YAG laser as the excitation line. The samples were loaded in Pyrex glass tubes (5 mm O.D.) under a dry argon atmosphere and sealed with a plastic cap. Infra-red spectra were obtained by an FT-IR spectrometer, FTS-155 (Bio-Rad Laboratories, Inc.). The sample was sandwiched between a pair of AgCl windows fixed in a stainless airtight cell. Ultraviolet-visible (UV-Vis) spectra were obtained by a Spectrophotometer, U-3010 (Hitachi High-Technologies Corp.). The samples were loaded in Pyrex glass tubes under a dry argon atmosphere and sealed with a plastic cap. Solvatochromic measurement was performed using the square planar complex salt, [Cu(tmen)(acac)][BPh$_4$] dissolved into the samples.[44, 45] The concentration of the complex was 0.01 M.

Quantum Mechanical Calculation. The Gaussian 03 program[46] was used for quantum mechanical calculations. Five calculation methods (HF, B3LYP, PBE1PBE, MPW1PW91, and MP2) combined with cc-pVTZ and aug-cc-pVTZ basis sets were used. The geometries of HOSO$_2$F, SO$_3$F$^-$, (FO$_2$SOH)$_2$O$_2$SOF$^-$, and SO$_3$CF$_3^-$ were optimized under C_1, C_{3v}, C_s, and C_{3v} symmetries. The geometry of (FO$_2$SOH)OSO$_2$F$^-$ was optimized at both C_1 and C_i symmetries since the results were highly dependent on method and basis set (see Results and discussion for details). Vibrational frequencies and intensities were calculated for the optimized geometries. Molecular volumes were calculated for the optimized geometries by the Monte Carlo method as implemented in Gaussian 03. The NBO analyses were performed for the B3LYP, PBE1PBE, and MPW1PW91 optimized local minima.[23-26]

Acknowledgements

References

1. J. S. Wilkes, *Green Chem.*, 2002, **4**, 73-80.

2. K. R. Seddon, *J. Chem. Technol. Biotechnol.*, 1997, **68**, 351-356.

3. P. Wasserscheid and W. Keim, *Angew. Chem. Int. Ed.*, 2000, **39**, 3772-3789.

4. R. Hagiwara and Y. Ito, *J. Fluorine Chem.*, 2000, **105**, 221-227.

5. T. Welton, *Chem. Rev.*, 1999, **99**, 2071-2083.

6. H. Xue, R. Verma and J. M. Shreeve, *J. Fluorine Chem.*, 2006, **127**, 159-176.

7. R. Hagiwara and J. S. Lee, *Electrochemistry*, 2007, **75**, 23-34.

8. H. Ohno, *Electrochemical Aspects of Ionic Liquids*, John Wiley and Sons, Inc., Hoboken, NJ, 2005.

9. J. S. Wilkes and M. J. Zaworotko, *J. Chem. Soc., Chem. Commun.*, 1992, 965-967.

10. E. I. Cooper and E. J. M. O'Sullivan, *Proceedings of the 8th International Symposium on Molten Salts*, 1992, 386-396.

11. K. Matsumoto, R. Hagiwara, R. Yoshida, Y. Ito, Z. Mazej, P. Benkic, B. Zemva, O. Tamada, H. Yoshino and S. Matsubara, *Dalton Trans.*, 2004, 144-149.

12. T. Nakajima, B. Zemva and A. Tressaud, *Advanced Inorganic Fluorides: Synthesis, Characterization, and Applications*, Elsevier Science S. A., Avenue de la Gare 50, 1003 Lausanne, Switzerland, 2000.

13. K. Matsumoto and R. Hagiwara, *Inorg. Chem.*, 2009, **48**, 7350-7358.

14. D. L. Zhang, S. J. Rettig, J. Trotter and F. Aubke, *Inorg. Chem.*, 1996, **35**, 6113-6130.

15. C. Josson, M. Deporcqstratmains and P. Vast, *Bull. Soc. Chim. Fr.*, 1977, 820-824.

16. A. Ruoff, J. B. Milne, G. Kaufmann and M. Leroy, *Z. Anorg. Allg. Chem.*, 1970, **372**, 119-126.

17. C. S. Alleyne, K. O. Mailer and R. C. Thompson, *Can. J. Chem.*, 1974, **52**, 336-342.

18. K. K. Laali and V. J. Gettwert, *J. Org. Chem.*, 2001, **66**, 35-40.

19.   R. Hagiwara, K. Matsumoto, Y. Nakamori, T. Tsuda, Y. Ito, H. Matsumoto and K. Momota, *J. Electrochem. Soc.*, 2003, **150**, D195-D199.

20.   Y. Yoshida, J. Fujii, K. Muroi, A. Otsuka, G. Saito, M. Takahashi and T. Yoko, *Synth. Met.*, 2005, **153**, 421-424.

21.   Y. Yoshida, K. Muroi, A. Otsuka, G. Saito, M. Takahashi and T. Yoko, *Inorg. Chem.*, 2004, **43**, 1458-1462.

22.   M. B. Herath, T. Hickman, S. E. Creager and D. D. DesMarteau, *J. Fluorine Chem.*, **132**, 52-56.

23.   A. E. Reed, R. B. Weinstock and F. Weinhold, *J. Chem. Phys.*, 1985, **83**, 735-746.

24.   A. E. Reed, L. A. Curtiss and F. Weinhold, *Chem. Rev.*, 1988, **88**, 899-926.

25.   E. D. Glendening, A. E. Reed, J. E. Carpenter and F. Weinhold, *NBO*, (1990) Gaussian, Inc., Pittsburgh, PA.

26.   E. D. Glendening, J. K. Badenhoop, A. E. Reed, J. E. Carpenter, C. M. Bohmann, C. M. Morales and F. Weinhold, *NBO*, (2001) Theoretical Chemistry Institute, University of Wisconsin, Madison, WI.

27.   Z. Pajaak, P. Czarnecki, H. Maluszynska, B. Szafranska and M. Szafran, *J. Chem. Phys.*, 2000, **113**, 848-853.

28.   J. Ohtsuki, K. Matsumoto and R. Hagiwara, *Electrochemistry*, 2009, **77**, 624-626.

29.   R. Hagiwara, T. Hirashige, T. Tsuda and Y. Ito, *J. Electrochem. Soc.*, 2002, **149**, D1-D6.

30.   H. Nakagawa, S. Izuchi, K. Kuwana, T. Nukuda and Y. Aihara, *J. Electrochem. Soc.*, 2003, **150**, A695-A700.

31.   C. A. Angell, N. Byrne and J. P. Belieres, *Acc. Chem. Res.*, 2007, **40**, 1228-1236.

32.   W. Xu, E. I. Cooper and C. A. Angell, *J. Phys. Chem. B*, 2003, **107**, 6170-6178.

33.   M. Yoshizawa, W. Xu and C. A. Angell, *J. Am. Chem. Soc.*, 2003, **125**, 15411-15419.

34.   T. Enomoto, Y. Nakamori, K. Matsumoto and R. Hagiwara, *J. Phys. Chem. C*, 2011, **115**, 4324-4332.

35. Y. Saito, K. Hirai, K. Matsumoto, R. Hagiwara and Y. Minamizaki, *J. Phys. Chem. B*, 2005, **109**, 2942-2948.

36. M. Y. Lui, L. Crowhurst, J. P. Hallett, P. A. Hunt, H. Niedermeyer and T. Welton, *Chem. Sci.*, 2011, **2**, 1491-1496.

37. H. Tokuda, S. Tsuzuki, M. Susan, K. Hayamizu and M. Watanabe, *J. Phys. Chem. B*, 2006, **110**, 19593-19600.

38. J. Fuller, R. T. Carlin and R. A. Osteryoung, *J. Electrochem. Soc.*, 1997, **144**, 3881-3886.

39. Y. Katayama, S. Dan, T. Miura and T. Kishi, *J. Electrochem. Soc.*, 2001, **148**, C102-C105.

40. V. R. Koch, L. A. Dominey, C. Nanjundiah and M. J. Ondrechen, *J. Electrochem. Soc.*, 1996, **143**, 798-803.

41. K. Matsumoto and R. Hagiwara, *J. Electrochem. Soc.*, 2010, **157**, A578-A581.

42. M. Ue, A. Murakami and S. Nakamura, *J. Electrochem. Soc.*, 2002, **149**, A1572-A1577.

43. P. Johansson, *J. Phys. Chem. A*, 2006, **110**, 12077-12080.

44. Y. Fukuda and K. Sone, *Bull. Chem. Soc. Jpn.*, 1972, **45**, 465-469.

45. R. W. Soukup and K. Sone, *Bull. Chem. Soc. Jpn.*, 1987, **60**, 2286-2288.

46. M. J. Frisch, G. W. Trucks, H. B. Schlegel, G. E. Scuseria, M. A. Robb, J. R. Cheeseman, J. J. A. Montgomery, T. Vreven, K. N. Kudin, J. C. Burant, J. M. Millam, S. S. Iyengar, J. Tomasi, V. Barone, B. Mennucci, M. Cossi, G. Scalmani, N. Rega, G. A. Petersson, H. Nakatsuji, M. Hada, M. Ehara, K. Toyota, R. Fukuda, J. Hasegawa, M. Ishida, T. Nakajima, Y. Honda, O. Kitao, H. Nakai, M. Klene, X. Li, J. E. Knox, H. P. Hratchian, J. B. Cross, V. Bakken, C. Adamo, J. Jaramillo, R. Gomperts, R. E. Stratmann, O. Yazyev, A. J. Austin, R. Cammi, C. Pomelli, J. W. Ochterski, P. Y. Ayala, K. Morokuma, G. A. Voth, P. Salvador, J. J. Dannenberg, V. G. Zakrzewski, S. Dapprich, A. D. Daniels, M. C. Strain, O. Farkas, D. K. Malick, A. D. Rabuck, K. Raghavachari, J. B. Foresman, J. V. O. Q. Cui, A. G. Baboul, S. Clifford, J. Cioslowski, B. B. Stefanov, G. Liu, A. Liashenko, P. Piskorz, I. Komaromi, R. L. Martin, D. J. Fox, T. Keith, M. A.

Al-Laham, C. Y. Peng, A. Nanayakkara, M. Challacombe, P. M. W. Gill, B. Johnson, W. Chen,

M. W. Wong, C. Gonzalez and J. A. Pople, *Gaussian 03*, (2003) Gaussian, Inc., Pittsburgh, PA.

Table of Contents (TOC) Image

Thermal, physical, and electrochemcial properties of fluorosulfate-based ionic liquids are reported. Molecular geometries of $(FO_2SOH)OSO_2F^-$ and $(FO_2SOH)_2O_2SOF^-$ in the ionic liquid states are discussed by means of quantum mechanical calculations.

SO_3F^- $(FO_2SOH)OSO_2F^-$

$(FO_2SOH)_2O_2SOF^-$